Biochemical and Biophysical Research Communications 679 (2023) 6–14

Contents lists available at ScienceDirect

Biochemical and Biophysical Research Communications

journal homepage: www.elsevier.com/locate/ybbrc

Active site serine-193 modulates activity of human aromatic amino acid decarboxylase

Giovanni Bisello [a,1], Giada Rossignoli [a,1,2], Sarah Choi [c], Robert S. Phillips [b,c,**], Mariarita Bertoldi [a,*]

[a] Section of Biochemistry, Department of Neuroscience, Biomedicine and Movement Sciences, University of Verona, Strada Le Grazie, 8, Verona, Italy
[b] Department of Chemistry, University of Georgia, Athens, GA, 30602, USA
[c] Department of Biochemistry and Molecular Biology, University of Georgia, Athens, GA, 30602, USA

ARTICLE INFO

Keywords:
Phosphorylation
Pyridoxal 5′-phosphate
Aromatic amino acid decarboxylase
Protein chemistry
Site-directed mutagenesis

ABSTRACT

Aromatic amino acid decarboxylase is a pyridoxal 5′-phosphate-dependent enzyme responsible for the synthesis of the neurotransmitters, dopamine and serotonin. Here, by a combination of bioinformatic predictions and analyses, phosphorylation assays, spectroscopic investigations and activity measurements, we determined that Ser-193, a conserved residue located at the active site, can be phosphorylated, increasing catalytic efficiency. In order to determine the molecular basis for this functional improvement, we determined the structural and kinetic properties of the site-directed variants S193A, S193D and S193E. While S193A retains 27% of the catalytic efficiency of wild-type, the two acidic side chain variants are impaired in catalysis with efficiencies of about 0.15% with respect to the wild-type. Thus, even if located at the active site, Ser-193 is not essential for enzyme activity. We advance the idea that this residue is fundamental for the correct architecture of the active site in terms of network of interactions triggering catalysis. This role has been compared with the properties of the Ser-194 of the highly homologous enzyme histidine decarboxylase whose catalytic loop is visible in the spatial structure, allowing us to propose the validation for the effect of the phosphorylation. The effect could be interesting for AADC deficiency, a rare monogenic disease, whose broad clinical phenotype could be also related to post translational AADC modifications.

1. Introduction

Aromatic amino acid decarboxylase (AADC) is a key enzyme involved in the synthesis of two essential neurotransmitters: dopamine and serotonin. Such a fundamental enzyme is hinged in metabolic pathways, leading to the formation of biogenic amines responsible for complex neurotransmitter networks [1]. Fig. 1 shows the dopaminergic and serotonergic pathways preceding and following AADC and the strictly correlated metabolic linkages. Such a finely tuned equilibrium among monoamine neurotransmitters necessitates of a deep regulative control. Indeed, an alteration in the levels of both dopamine and serotonin leads to severe motor and psychiatric disorders such as Parkinson's disease (PD) [2] or AADC deficiency, a form of infantile parkinsonism of genetic origin [3]. Given the fundamental role played by AADC in neurometabolic pathways, it is curious that few data exist concerning its regulation, especially at the protein level. The gene coding for AADC maps on chromosome 7p12.2-p12.1 [4] and is organized in 15 exons, with two alternative first exons. Two tissue-specific transcripts, one of neuronal and the other of non-neuronal origin, under the control of their respective promoters, are synthesized [5–8]. The group of Vassilacopoulou produced evidence for the presence of the neuronal mRNA also in non-neuronal tissues, namely liver, kidney, placenta and leukocytes ([9] and references therein). In terms of transcription, some transcription factors and regulators of chromatin remodeling have been claimed to play a role in AADC neuronal promoter binding [10–12] producing a ternary complex with two neuronal transcription factors present in nerve cells during de-differentiation, thus launching the interesting idea that this biological activity is under control targeting *DDC* gene expression [10].

* Corresponding author.
** Corresponding author. Department of Chemistry, University of Georgia, Athens, GA, 30602, USA.
E-mail addresses: plp@uga.edu (R.S. Phillips), mita.bertoldi@univr.it (M. Bertoldi).
[1] first co-authors.
[2] Current affiliation: Department of Biology, University of Padua, Padua, Italy

https://doi.org/10.1016/j.bbrc.2023.08.049
Received 29 June 2023; Received in revised form 8 August 2023; Accepted 22 August 2023
Available online 23 August 2023

Abbreviations

PLP	pyridoxal 5′-phosphate
PMP	pyridoxamine 5′-phosphate
AADC	aromatic amino acid decarboxylase
HDC	histidine decarboxylase
WT	wild-type
Tm	melting temperature
CD	circular dichroism
PD	Parkinson's disease
PKA	protein kinase A

Considering possible regulation in terms of gene expression, alterations are reported in several neurodegenerative and psychiatric disorders and are present in neoplasia. A search into the PubMed database reveals more than 200 reports relating *DDC* gene expression and several forms of tumors, such as the recent reports [13–15], reaffirming the relevance of neurotransmitter metabolism in cancer.

As far as the protein is concerned, it was reported that stimulation or blockade of dopamine receptors may influence AADC activity in the striatum [16–19]. In addition, vesicular monoamine transporter-2 (VMAT-2) has been demonstrated to physically and functionally interact with AADC, and also with tyrosine hydroxylase, to couple dopamine synthesis to transport into vesicles [20]. This interaction is reminiscent of another protein-protein interaction study between AADC and DJ1, the causative protein for the familial PD [21]. Moreover, a functional interplay of α-synuclein with AADC has been advanced in the context of the control of dopamine levels, which is lost in PD [22].

In addition to these scattered data, we recently reviewed [23] that AADC can be phosphorylated by both cyclic AMP-dependent kinase (PKA) [24] and cyclic GMP-protein kinase G [25]. In both cases, phosphorylation results in an increase in decarboxylase activity. However, this aspect should be more deeply investigated with special regard to the pathological states in which AADC is involved. No reports are present in the literature correlating the phosphorylation state and AADC modification to the severity or the mildness of either PD or AADC deficiency. A better understanding of the molecular effects induced by phosphorylation on the AADC protein is thus desirable.

Here, we carried out bioinformatic analyses to map possible phosphorylation sites of AADC, performed phosphorylation stimulation assays by using recombinant human AADC or histidine decarboxylase (HDC), a highly homologous enzyme, as substrate, and identified a possible target residue interestingly located at the active site. In order to dissect the role of the residue subjected to modification, we characterized some site-directed variants and proposed a possible contribution for phosphorylation in regulating AADC activity.

2. Materials and methods

2.1. Materials

All chemicals and reagents were purchased from internationally established companies and were of the highest purity available.

2.2. Wild-type (WT) and AADC variants, WT HDC and PKA cloning, expression and purification

WT AADC has been expressed and purified as reported [26]. The enzyme concentration was determined using an ε_M of 1.42×10^5 M^{-1}

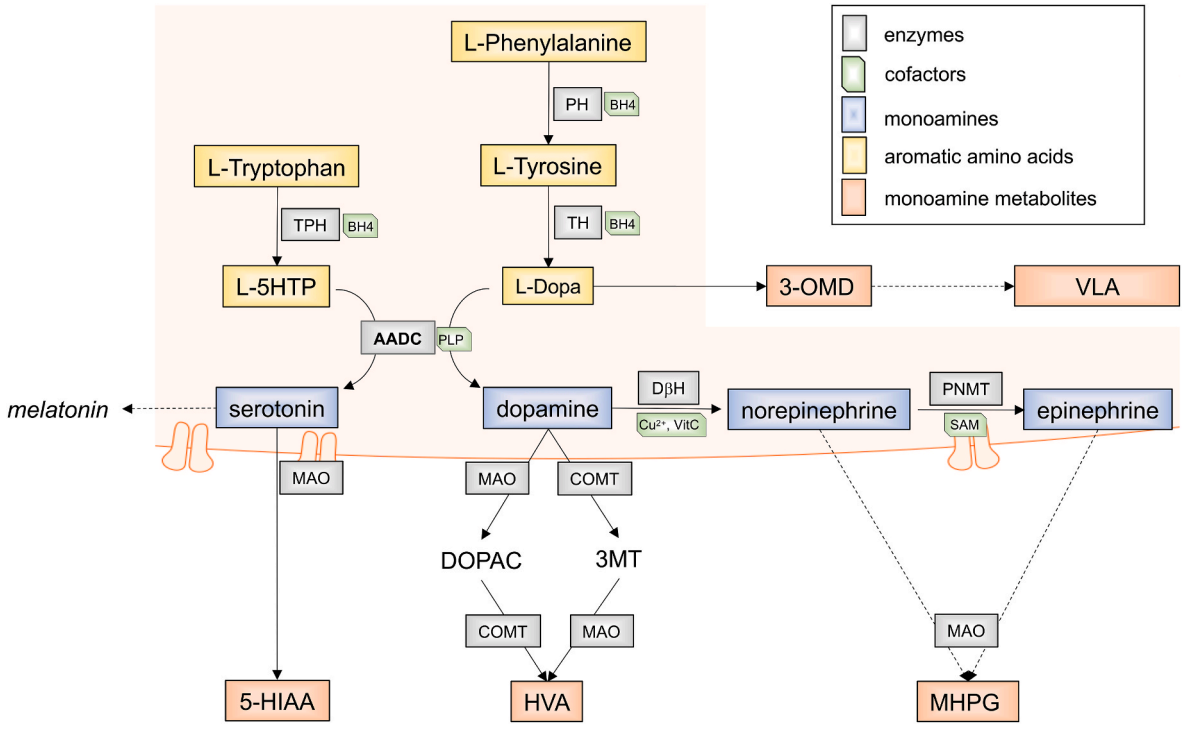

Fig. 1. Metabolic networks involving AADC. The intertwined networks in which AADC is involved in cells. Aromatic amino acids are in yellow (L-Phenylalanine, L-Tyrosine, L-Tryptophan, L-Dopa and L-5-hydroxytryptophan, L-5HTP); their metabolic derivatives, hallmarks for AADC deficiency, are in orange (3-O-methyldopa, 3-OMD; vanillactic acid, VLA; homovanillic acid, HVA; 5-hydroxyindoleacetic acid, 5-HIAA, 3-methoxy 4-hydroxyphenylglycol, MHPG); other derivatives (dihydroxyphenylacetic acid, DOPAC; 3-methoxytyramine, 3-MT) are white; aromatic monoamines are in blue (dopamine, serotonin, norepinephrin, epinephrin); enzymes are in grey (AADC; dopamine beta hydroxylase, DβH; phenylalanine hydroxylase, PH; tyrosine hydroxylase, TH; tryptophan hydroxylase, TPH; catechol O-methyl transferase, COMT; monoamine oxidase, MAO); their respective cofactors (tetrahydrobiopterin, BH4; PLP; cupper, Cu; vitamin C) and methyl donor (S-adenosylmethionine, SAM) in green. (For interpretation of the references to colour in this figure legend, the reader is referred to the Web version of this article.)

cm^{-1} at 280 nm. Pyridoxal 5′-phosphate (PLP) content was determined by releasing the coenzyme in 0.1 M NaOH using ε_M of 6600 M^{-1} cm^{-1} at 388 nm [27]. AADC variants were obtained by mutating the template DNA on the pDDChis vector as previously described [26]. Each mutagenesis reaction has been performed using the Quick-Change II kit (Agilent technologies) using the appropriate oligonucleotides (5′-CCGATCAGGCACACGACTCAGTGGAAAGAG-3′ for S193D and 5′-CATCCGATCAGGCACACGAGTCAGTGGAAA-3′ for S193E, and 5′-CCGATCAGGCACACGCCTCAGTGGAAAGAG-3'for S193A, and their complements. The modified bases are underlined). All mutations were confirmed by DNA sequence analysis of the whole ORF. The catalytic subunit of mouse protein kinase A was expressed in *E. coli* BL21(DE3) cells containing pRSETB/PKA (a generous gift of Professor Eileen Kennedy of the Department of Pharmaceutical Sciences of the University of Georgia) grown in Studier autoinduction medium [28]. Protein production by auto-induction in high-density shaking cultures [28] was performed at 37 °C. The enzyme was purified from cell free extracts by chromatography with phosphocellulose P-11 [29].

2.3. Determination of the apparent equilibrium dissociation constant for PLP in WT AADC and its variants and measurement of the kinetic parameters for all AADC species and WT HDC

AADC apoenzyme was obtained by incubating 5 μM holoenzyme with 10 mM hydroxylamine in 0.5 M potassium phosphate buffer pH 6.8 at 25 °C for 3 h. The solution was then loaded on a Desalting 26/10 column (GE Healthcare) preequilibrated with 0.5 M potassium phosphate buffer pH 6.8 and eluted at 1 mL/min. The eluted enzyme was then concentrated on an Amicon Ultra 15 concentrator (Millipore) and washed with 100 mM potassium phosphate buffer pH 7.4. The apparent equilibrium dissociation constant for PLP, $K_{D(PLP)}$, for all AADC species was determined by measuring the quenching of the intrinsic fluorescence of 0.1 μM AADC apoenzyme incubated in the presence of PLP at concentrations ranging from 0.005 to 20 μM for 3 h at 25 °C (in the dark) in 100 mM potassium phosphate buffer pH 7.4. The data were fitted to the following equation:

$$Y = Y_{MAX}\left([E]_t + [PLP]_t + K_{D(PLP)} - \frac{\sqrt{\left([E]|t + [PLP]_t + K_{D(PLP)}\right)^2 - 4[E]_t[PLP]_t}}{2[E]_t}\right)$$

where $[E]_t$ and $[PLP]_t$ represent the total concentrations of the enzyme and PLP, respectively, Y refers to the intrinsic quenching changes at a PLP concentration, and Y_{max} refers to the fluorescence changes when all enzyme molecules are complexed with coenzyme. Curve fitting was performed using Prism, 8.4.0 (GraphPad).

2.4. Decarboxylase assays and determination of coenzyme derivatives by HPLC

The AADC decarboxylase activity was measured by a discontinuous spectrophotometric assay, as described [30,31]. WT AADC or S193A variant (0.1 μM concentration for both) was incubated for 1 h under saturating PLP concentration (10 μM) and different L-Dopa concentrations (from 0.025 to 3 mM) were added in a final volume of 250 μL in 100 mM potassium phosphate buffer pH 7.4 for a time within which a linear product formation is observed. WT HDC was incubated for 1 h under saturating PLP concentration (10 μM) and different L-histidine concentrations in a final volume of 250 μL in 100 mM potassium phosphate buffer pH 7.4 for a time within which a linear product formation is observed, as reported in Ref. [32]. Thereafter, the procedure is identical for the two decarboxylases. The reaction was then stopped by heating at 100 °C for 2 min. Trinitrobenzene sulfonic acid (1 ml of a 4.3 mM solution) and toluene (1.5 ml) were added and the extraction of trinitrophenyl-derivative was carried out at 42 °C for 45 min with continuous shaking. The concentration of trinitrophenyl-derivative in the toluene layer was quantified using a prepared calibration curve of absorbance at 340 nm as a function of trinitrophenyl-derivative concentration [31]. In the case of variants (S193D and S193E) forming dopamine below the detection limit of the spectrophotometric assay, kinetic parameters were determined by HPLC with an already published procedure [33]. Each enzyme (at 5 μM concentration) was incubated in the presence of 100 μM PLP and different L-Dopa concentrations (from 0.025 to 4 mM) in a final volume of 225 μL in 100 mM potassium phosphate buffer pH 7.4 for a time within which a linear product formation is observed. The reactions were quenched by adding 25 μL of a 100% trichloroacetic acid solution. Proteins were precipitated in ice and removed by centrifugation. Supernatants were analyzed by using a Gemini C18 column (150 × 4.6 mm, Phenomenex, CA, USA) on a Jasco PU-2080 Plus HPLC system equipped with a UV-1570 detector set at 295 nm. Samples were eluted in 50 mM potassium phosphate, pH 2.35, at a flow rate of 1 mL/min. Standard curves of dopamine peak area as well as PLP, PMP, and Pictet-Spengler cyclic adduct were prepared as reported [33] with commercially available compounds. The cyclic adduct was synthesized by completely reacting free PLP with L-Dopa and purifying it by HPLC. The kinetic parameters were determined by fitting the data obtained to the Michaelis-Menten equation by non-linear regression analysis using Prism, 8.4.0 (GraphPad).

2.5. Phosphorylation assays

Phosphorylation assays were performed in a thermostatic bath at 37 °C for 30 min. The standard phosphorylation mix was composed by 50 mM Tris-HCl pH 7.5, 1 mM $MgCl_2$, 1 mM ATP, and 1:10 ratio between AADC or HDC and the catalytically active PKA. The kinetic parameters of AADC and HDC were then calculated by adding an aliquot of this mixture to a typical assay solution, as described [30–32]. Controls with untreated AADC and HDC in the same experimental conditions were carried out.

2.6. Bioinformatic predictions and analyses

Bioinformatic predictions of AADC and HDC for possible phosphorylation sites were performed using NetPhos 3.1 free online server (http://www.cbs.dtu.dk/services/NetPhos) using the corresponding amino acid sequence of the cloned gene.

For i*n silico* amino acid substitution analyses human AADC sequence (EC: 4.1.1.28) was aligned with 75 homologs sequences retrieved from Uniref-90 database by the homolog search algorithm PSI-BLAST and aligned using Multiple Sequence Alignment software CLUSTALW on ConSurf server (http://consurf.tau.ac.il). A conservation score (9 = conserved, 1 = variable) was attributed to each residue. Structural analysis of AADC and HDC was carried out using Pymol 2.2.3 (The PyMOL Molecular Graphics System, Version 2.0 Schrödinger, LLC) using the PDB coordinates 1JS3 and 4E1O, respectively. BindProfX was used to predict changes in binding affinity upon mutations in the form of ΔΔG (change in free energy of binding) values. The algorithm combines the FoldX physics-based potential with the conservation scores from pairs of protein-protein interaction surfaces sequence profiles.

2.7. Mass spectrometry

AADC was incubated with PKA as described above. The phosphorylated protein was then run on a polyacrylamide gel. After staining with Comassie Blue, the AADC band was cut from the gel. The gel bands were sliced into small pieces, and then rinsed with 50% acetonitrile/20 mM ammonium bicarbonate (~pH 7.5–8) twice. The gel pieces were dehydrated by adding 100% of acetonitrile and dried out by a SpeedVac. A various amount of Trypsin solution (0.01 μg/μL in 20 mM ammonium bicarbonate) was added until the gel pieces totally absorb the Trypsin solution. The tubes were placed in an incubator at 37 °C overnight. The tryptic peptides were extracted from gel pieces by incubating with 50%

acetonitrile/0.1% formic acid twice. The extracts were dried down by a SpeedVac.

The mass spectrometry analyses were performed on a Thermo-Fisher LTQ Orbitrap Elite Mass Spectrometer coupled with a Proxeon Easy NanoLC system (Waltham, MA) located at Proteomics and Mass Spectrometry Facility, University of Georgia. The enzymatic peptides were loaded into a reversed-phase column (self-packed column/emitter with 200 Å 5 μM Bruker MagicAQ C18 resin), then directly eluted into the mass spectrometer. Briefly, the two-buffer gradient elution (0.1% formic acid as buffer A and 99.9% acetonitrile with 0.1% formic acid as buffer B) starts with 0% B, holds at 0%B for 2 min, then increases to 30% B in 50 min, to 50% B in 10 min, and to 95% B in 10 min.

The data-dependent acquisition (DDA) method was used to acquire MS data. A survey MS scan was acquired first, and then the top 8 ions in the MS scan were selected for following CID MS/MS analysis. Both MS and MS/MS scans were acquired by Orbitrap at the resolutions of 120,000 and 15,000, respectively.

Data were acquired using Xcalibur software (version 2.2, Thermo Fisher Scientific). Proteins identification and modification characterization were performed using Thermo Proteome Discoverer (version 1.4) with Mascot (Matrix Science) and Uniprot database. The spectra of possible modified peptides were inspected further to verify the accuracy of the assignments.

2.8. Spectroscopic measurements and melting temperature determination

All spectroscopic measurements were acquired in 100 mM potassium phosphate, pH 7.4, at 25 °C. CD measurements were recorded with a Jasco J-710 spectropolarimeter at a scan speed of 50 nm/min with a bandwidth of 2 nm at a protein concentration of 1–5 μM. Thermal denaturation was performed by monitoring the CD signal at 222 nm of 4 μM enzyme on a 25–90 °C linear temperature gradient, with a temperature slope of 1 °C/min. Exogenous PLP (100 μM) was added to the holoenzymes. Analysis of the internal and external aldimine spectral modifications has been carried out on a Jasco V-550 spectrophotometer at a protein concentration of 5 μM in the absence or in the presence of saturating concentration (2 mM) of the substrate analog dopa methylester (DME) and of L-Dopa.

3. Results and discussion

3.1. Bioinformatic analysis and mass spectrometry reveal that Ser-193 is an active site phosphorylation target of AADC

A search in the database predicts multiple potential phosphorylation sites of AADC (Table 1) for many different kinases, including PKA, protein kinase C (PKC), cell cycle control protein kinase 2 (cdc2), casein kinase 2 (CK2), and p38 mitogen-activated protein kinases (p38MAPK).

Following previous reports in the literature [24,25], our attention was focused on PKA and PKC predicted phosphorylation sites. The position of the target residues in the enzyme structures was analyzed, in order to eliminate those located in the protein core or solvent inaccessible. Among the putative target sites, some of them (Ser-104, Ser-193 and Thr-323) are located at or in proximity to the active site (Fig. 2).

Table 1
Predicted phosphorylation sites of AADC.

Enzyme	Kinase	NetPhos score	Amino acid
AADC	PKA	0.757	Ser220
		0.722	Ser416
		0.663	Thr320
	PKC	0.764	Thr323
		0.711	Ser193
		0.694	Ser104
		0.583	Ser429

The underlined residues are located at or in proximity to the active site.

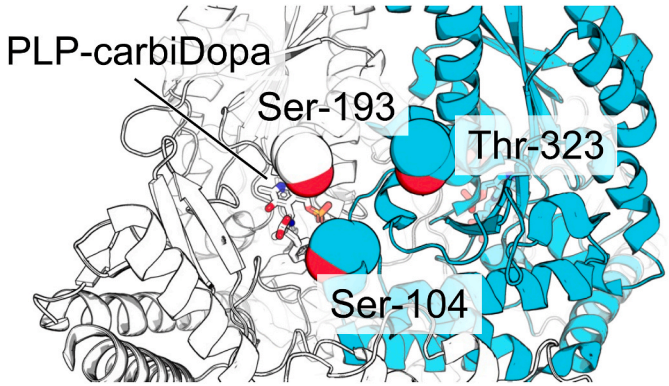

Fig. 2. Visualization of the predicted phosphorylation sites of AADC. Predicted phosphorylation sites on AADC. Dimeric porcine AADC (pdb: 1js3) is represented as cartoon and the two subunits are coloured white and cyan respectively. The complex pyridoxal PLP-carbidopa is shown as sticks while the putative phosphorylation sites are shown as spheres, in red the hydroxyl groups. (For interpretation of the references to colour in this figure legend, the reader is referred to the Web version of this article.)

The *in vitro* phosphorylation assay mixture (prepared as reported in Materials and Methods) was sent to the *Proteomics and Mass Spectrometry Core Facility* of the University of Georgia (Athens, Georgia, USA) to identify the involved residue(s). A tryptic peptide with the sequence LVAYSSDQAH(S)SVER was identified by mass spectrometry as phosphorylated on Ser-193 in about 15% of AADC protein. A separate experiment was performed, and the same peptide was again found to be phosphorylated. In the second experiment, Ser-312 was found to be phosphorylated at a low level, in addition to Ser-193 (Tables S1 and S2). However, Ser-312 is not predicted as a phosphorylation site and is buried. The low phosphate incorporation could be due to the lability of the phosphorylated serine during gel electrophoresis, tryptic digestion, or mass spectrometry or to differences in ionization efficiency. It is not surprising that this serine residue, predicted as a phosphorylation site for PKC, has been found phosphorylated following PKA stimulation, given the similarity of the consensus sequence of the two kinases requiring both basic amino acids close to the target serine on the substrate. It is also interesting that several Met residues were consistently found to be oxidized partially to sulfoxide (Tables S1 and S2).

Ser-193 is located at the active site of AADC at the dimeric interface (Fig. 3A) and immediately follows His-192, an essential residue [34,35] responsible for a stacking interaction with the pyridine ring of the cofactor. Ser-193 is conserved among homologous proteins (conservation score of 9, ConSurf server; http://consurf.tau.ac.il). Its polar side chain does not seem to be involved in any interaction; however, it is in close vicinity to several residues located on loop3 (Arg-347′, Leu-353’, the prime denotes residues belonging to the opposite subunit), a structurally flexible element responsible for the enzymatic activity of AADC, since it comprises the catalytic loop (residues 328-339 [35]) bearing the catalytic Tyr-332 [36]. Both Arg-347 and Leu-353 are substituted in AADC deficiency, giving rise to R347Q, R347G, and L353P variants whose molecular basis for the catalytical impairment has been already investigated [26,37,38]. Interestingly, Leu-353 is immediately preceding Gly-354, a residue suggested to control substrate preference in the homologous HDC where it is replaced by a Ser residue [39].

3.2. Phosphorylation of Ser-193 enhances the catalytic efficiency of L-Dopa and L-5-hydroxytryptophan decarboxylation

AADC has been incubated with PKA as reported in the Materials and Methods section in order to ensure total phosphorylation and then assayed for decarboxylase activity. As shown in Table 2, L-Dopa decarboxylation takes place with an increased catalytic efficiency mainly due

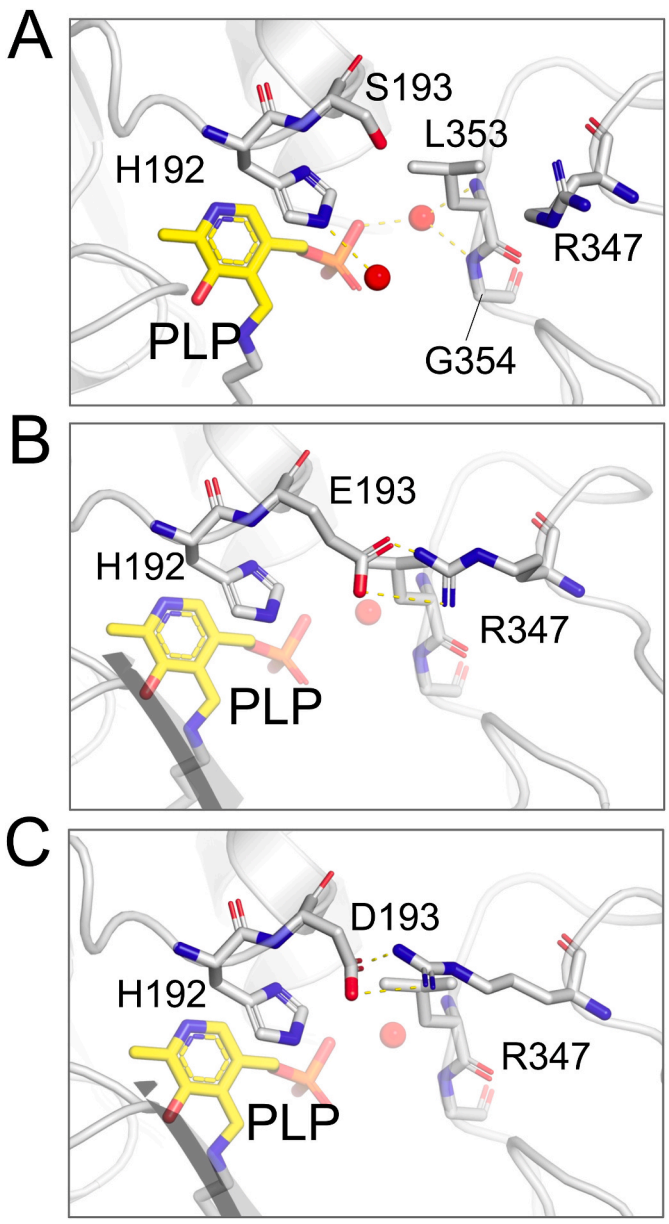

Fig. 3. Localization of Ser-193 and proposed effect of S193D and S193E on AADC active site. A) Ser-193 is located at the active site and its side chain is near His-192 engaged in a stacking interaction with the pyridine ring of PLP. *In silico* mutagenesis suggests that Asp (B) and Glu (C) variants could interact with Arg-347′ of the facing subunit, already observed to be highly sensitive to slight alterations of the active site.

Table 2
Kinetic parameters of phosphorylated AADC (AADC-P) in the presence of L-Dopa and L-5-hydroxytryptophan.

	L-dopa			L-5-hydroxytryptophan		
	k_{cat} (s^{-1})	K_m (mM)	k_{cat}/K_m (s^{-1} mM^{-1})	k_{cat} (s^{-1})	K_m (mM)	k_{cat}/K_m (s^{-1} mM^{-1})
AADC	7.4 ± 0.2	0.11 ± 0.01	67 ± 6	1.01 ± 0.02	0.038 ± 0.007	27 ± 5
AADC-P	8.6 ± 0.3	0.032 ± 0.009	269 ± 76	1.10 ± 0.07	0.013 ± 0.004	85 ± 27

to K_m decrease. Previous data collected on brain homogenates [25] exhibited a slight increase of both V_{max} and K_m leading to an about 87% of the catalytic efficiency of the sample not treated with protein kinase. This slightly different effect is possibly due to different assay conditions and samples.

The remarkable effect of recombinant AADC with L-Dopa is also mirrored by assaying decarboxylase activity of the other substrate, L-5-hydroxytryptophan, where the calculated catalytic efficiency results in this case increased by about 3-fold. Indeed, this enhancement is mainly driven, again, by an increase in substrate affinity. One could speculate on how the binding of the phosphate moiety at the active site could have produced such positive regulation. In order to determine the relevance of a negative charge (as introduced with phosphorylation) in this position we built and characterized site-directed variants of Ser-193.

3.3. Ser-193 AADC variants are affected in catalysis but not in structural signals

The S193A, S193D and S193E variants were generated in order to dissect how a modification of the hydroxy group of Ser-193 impacts on AADC activity. While the substitution with Ala totally withdraws the polarity, the change with acidic side chains, as in Asp and Glu, would mimic the negative charge of the phosphate moiety. The measured ΔΔG values are 0.798, 1.052 and 0.955 (calculated with BindProfX server, see Materials and Methods section), respectively, indicating that a negative charge or a change in side chain length or both introduce a destabilization of the interface. Since the two active sites are facing each other at the interface, this result predicts a negative effect on activity. It is already known that pathogenic variants, such as those identified in AADC deficiency, mapping at the interface have deleterious effects in terms of catalytic competence of AADC [26]. A bioinformatic inspection of the substitution of Ser-193 with Asp or Glu (Fig. 3B and 3C) shows, in both cases, a rearrangement of residues at the active site leading the new inserted negative charge to interact and displace Arg-347′ whose role in AADC catalysis has been recently clarified [38]. The subtle movement of Arg-347′ determines a restriction of the crevice at the active site [38] where Gly-354' may control substrate selectivity. In addition, this alteration at the active site determines a small change in the network of contacts of His-192. It has been already demonstrated that this residue is of particular importance for AADC [34] and other homologous decarboxylases [40], since it base stacks with the aromatic ring of the pyridine cofactor. In fact, its substitution leads to almost complete loss of activity. The substitution of Ser-193 does not lead to an altered equilibrium binding constant for the coenzyme, thus indicating that the alteration of the network with His-192 is not so severe in terms of PLP location. Instead, the catalytic kinetic parameters display a difference (Table 3).

While substitution of Ser-193 with Ala slightly decreases the k_{cat} keeping the K_m substantially unchanged, both S193D and S193E exhibit a severe drop in k_{cat} (resulting in 0.4% and 0.3% with respect to the WT and an increase in K_m (about 2.8-2.3-fold). In order to understand the molecular basis for the catalytic incompetence of the negatively charged variants we performed an extensive structural characterization. The far-UV CD spectra do not show differences with respect to the WT, substantiating that there are no gross structural alterations (Fig. 4A) in the secondary structure elements.

Table 3
Kinetic parameters and equilibrium dissociation constant for PLP of AADC Ser-193 variants.

Enzyme	k_{cat} (s^{-1})	K_m (mM)	k_{cat}/K_m (s^{-1} mM^{-1})	$K_{D(PLP)}$ (nM)
WT	7.4 ± 0.2	0.11 ± 0.01	67 ± 6	101 ± 10[a]
S193A	1.8 ± 0.1	0.096 ± 0.020	18 ± 5	92 ± 10
S193D	0.032 ± 0.001	0.31 ± 0.04	0.103 ± 0.004	84 ± 10
S193E	0.026 ± 0.001	0.25 ± 0.03	0.104 ± 0.004	98 ± 13

[a] As reported in [41].

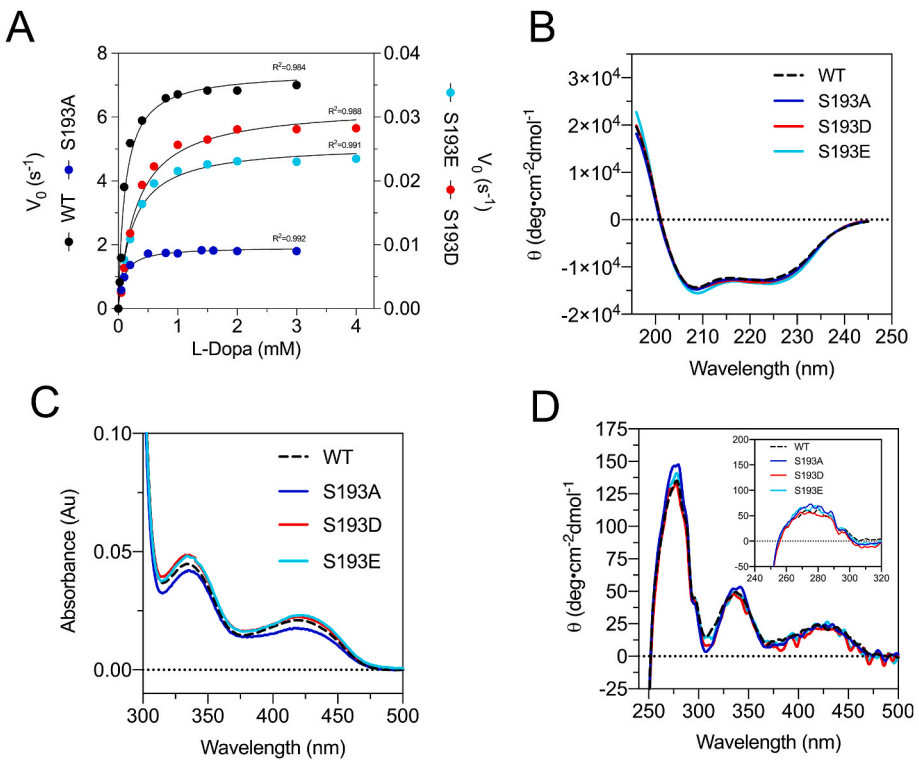

Fig. 4. Kinetic and spectroscopic features of apo and holo WT and Ser-variants. Kinetic and spectral characterization of S193A, S193D and S193E variants. A) Initial velocity values (nmol dopamine/time/nmol enzyme) on L-Dopa concentration have been measured and the experimental values have been fitted to the Michaelis-Menten model for each AADC species. R^2 value is shown for each fit. B) Far-UV CD spectra of holo variants compared to holoWT. Enzyme concentration was 1 mM in 100 mM potassium phosphate buffer, pH 7.4 in the presence of 100 μM PLP; C) Near-UV visible CD spectra of holo variants compared to holoWT. Spectra of the apo species are reported in the inset. CD spectra are recorded at 5 μM protein concentration, in 100 mM potassium-phosphate buffer, pH 7.4, in presence of 100 μM PLP for the holo forms. D) Absorbance spectra of holoWT and variants recorded at 5 μM protein concentration for all species, in 100 mM potassium-phosphate buffer, pH 7.4.

The thermal stability, Tm, measured as the dependence of the dichroic signal at 222 nm as a function of temperature, shows that the S193A variant is as stable as the WT, while both apo and holo species of the negatively charged variants are slightly more stable than the WT (Table 4).

Near-UV and visible CD (Fig. 4B), as well as absorbance spectra (Fig. 4C), show no alterations in tertiary structure of both apo and holo forms of all species with respect to the WT and a similar tautomeric equilibrium of the internal aldimine, with a predominance of the enolimine over the ketoenamine, as for the WT. The formation of the external aldimine has been monitored by adding the substrate analog DME to the enzymatic solutions (Fig. 5A). This analog is unable to undergo decarboxylation and can be used as a probe for integrity of active site microenvironment. While it was known that the addition of DME to WT AADC gives rise to a band at 395 nm (indicative of the external aldimine) that remains unaltered with time [41,42], both S193D and S193E in presence of DME show spectral modifications within 30 min consistent with the formation of the external aldimine, peaking at 395 nm, and the observable 500 nm band relative to an equilibrium between the external aldimine and a quinonoid species. This species has been demonstrated to occur when the Cα-proton of a compound (amine or substrate analog) bound to AADC is placed perpendicular [43] to the pyridine-imine plane, and in the correct position to be removed, giving rise to the oxidative deamination reaction that forms a ketimine intermediate (pyridoxamine 5′-phosphate (PMP) + carbonylic product) observable as an increase at 330 nm [44,45]. It is well known that PLP-dependent enzymes are able to catalyze side reactions, in addition to their main catalytic activities, given the extraordinary versatility of their cofactor [46,47]. The fact that a quinonoid species appears in the presence of DME with S193D and S193E suggests that the amino acid substitution with a negative residue has determined a subtle alteration at the active site, already visible following bioinformatic analyses, and thus confirmed by spectral data displaying an incorrect placement of the external aldimine intermediate.

When L-Dopa is added to a reaction mixture containing S193D and S193E, a modification of the spectrum of the internal aldimine occurs. At first, there is an increase of the 420 nm band and a shift of the 335 nm band to 329 nm. Then, more slowly, the 420 nm absorbance decreases and the 329 nm band increases (Fig. 5B). The HPLC analyses of both mixtures show that the coenzyme content remains almost unchanged during 1h being only slightly converted into the unproductive cyclic adduct of Pictet-Spengler and PMP, as the WT [33,48] (Fig. 5C). Thus, the slow dopamine formation is not attributable to the total conversion of the coenzyme into the irreversible cyclic adduct during reaction with L-Dopa, as it occurs with some AADC deficiency variants [26].

Table 4
Tm values of apo and holo forms of Ser-193 variants at 222 nm.

Enzyme	Tm (°C)	
	holo	apo
WT	69.42 ± 0.02	64.84 ± 0.03
S193A	69.09 ± 0.02	65.08 ± 0.03
S193D	70.67 ± 0.02	67.55 ± 0.03
S193E	70.69 ± 0.02	66.85 ± 0.04

3.4. *The homologous HDC is phosphorylated on Ser-194 and catalytically enhanced*

Ser-194 in HDC is, as with AADC, predicted by bioinformatic analysis as a putative phosphorylation target. Determination of the kinetic parameters following incubation with the phosphorylation mixture and then isolation of the enzyme (see Materials and Methods) shows that reduced HDC (the enzyme species more similar to the redox state of AADC, since it has recently been demonstrated that HDC exists as an equilibrium of mixture of reduced and oxidized species depending on the redox conditions [32]), has a similar behavior in terms of the effects carried out by phosphorylation (Table 5). Precisely, k_{cat} increases by a factor of 1.5 and K_m decreases by a factor of 2, making overall catalytic efficiency (k_{cat}/K_m) increase about 3-fold. This effect induced by phosphorylation confirms the trend demonstrated by AADC in response to a phosphorylation stimulus.

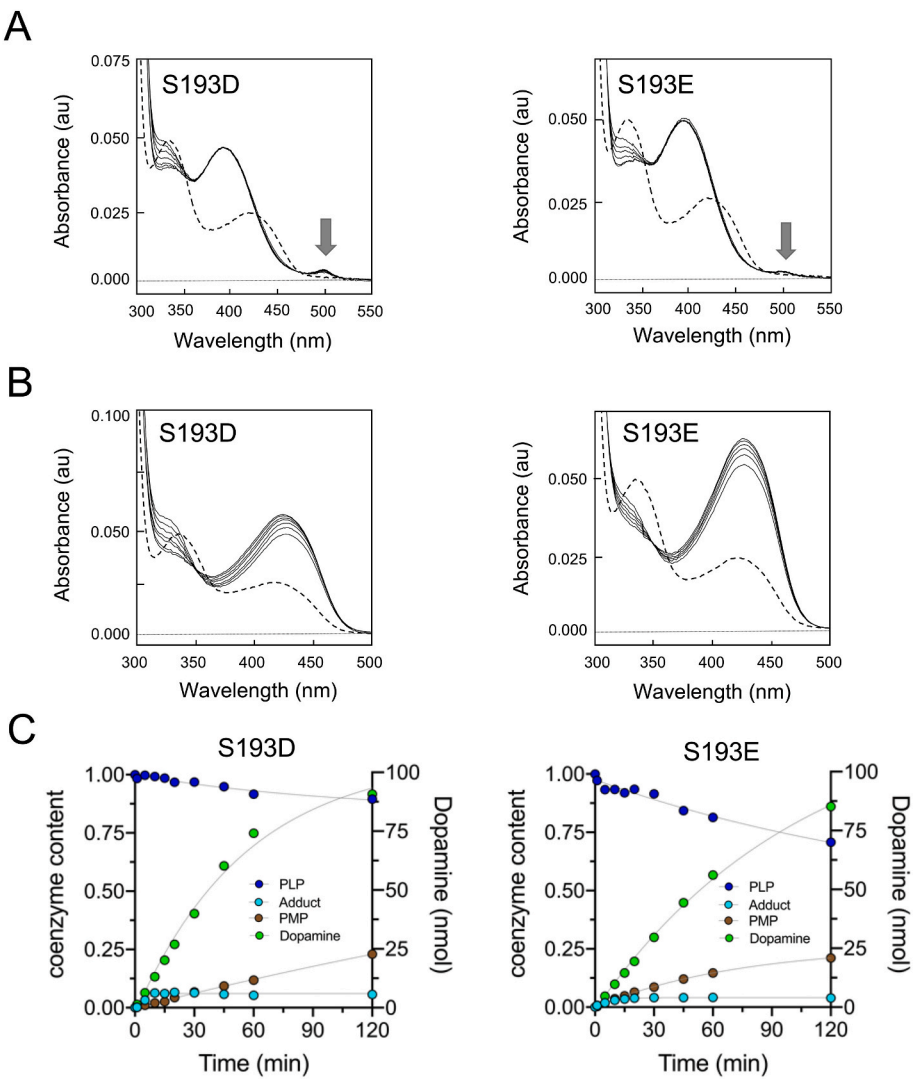

Fig. 5. Spectral changes of incubation mixtures of S193D or S193E in the absence or presence of DME and L-Dopa and HPLC analysis of coenzyme modifications in the presence of L-Dopa.
A) Absorbance spectra of 5 μM S193D and S193E variants in the presence of 2 mM DME in 100 mM potassium phosphate, pH 7.4 at 25 C during 30 min of reaction time. Dashed lines represent the spectra of the protein recorded in absence of substrate. The quinonoid species is indicated with an arrow; B) Absorbance spectra of 5 μM S193D and S193E variants in presence of 2 mM L-Dopa in 100 mM potassium phosphate, pH 7.4 at 25 C during 30 min of reaction time. Dashed lines represent the spectra of the protein recorded in absence of substrate; C) HPLC analysis of the reaction mixtures of 10 μM S193D and S193E variants in the presence of 2 mM L-Dopa. Coenzyme species (PLP, PMP or Pictet-Spengler cyclic adduct) and dopamine formation are plotted at different times as reported under the *Materials and Methods* section.

Table 5
Kinetic parameters of phosphorylated HDC (HDC-P) in the presence of L-histidine.

	L-histidine		
	k_{cat} (s^{-1})	K_m (mM)	k_{cat}/K_m (s^{-1} mM^{-1})
redHDC	0.70 ± 0.02[a]	0.064 ± 0.008 [a]	10.9 ± 1.4[a]
redHDC-P	1.03 ± 0.02	0.032 ± 0.004	32.19 ± 4.07

[a] As reported in [32].

3.5. Role of AADC Ser-193 in the absence or presence of bound phosphate

The collected data regarding AADC Ser-193 variants indicate that this conserved residue located at the active site does not play a crucial role in catalysis, since the functional abilities of S193A are only slightly affected. The combination of bioinformatic analyses, spectroscopic and kinetic data, measured with S193D and S193E, provides evidence that novel inter-subunit interactions between Asp or Glu-193 and Arg-347' would contribute in anchoring loop3 in a sort of fixed conformation. Since loop3 includes the mobile catalytic loop [35] and this stretch contains the catalytic Tyr-332 residue [36], this interaction may be related to the although small but measurable increased stability evidenced by higher Tm values and could account for the drop in catalytic efficiency. Furthermore, in the homologous HDC we have observed a similar kinetic behavior in the presence of PKA. Interestingly, the catalytic HDC Tyr-334 (Tyr-332 in AADC) has been seen to interact with Ser-195 of the other subunit (Ser-194 in AADC), thus the substitution of the preceding HDC Ser-194 (Ser-193 in AADC) could disassemble some required interaction network necessary for catalytic competence.

In any case, the question remains open: How could phosphorylation by PKA decrease the K_m and increase k_{cat}? Our data seem to reject that these results are due to the presence of the negative charge, unless we propose that a polyanion (as in the phosphate anion but not in the carboxylate one) could give rise to different behavior than a single negative charge. The spatial structure [35] shows that Ser-193 is in close proximity to His-192, an essential residue to stack with the pyridine ring of the PLP cofactor, and keeping it in the correct position. In addition, Ser-193 belongs to a region where the catalytic loop, invisible in the electron density map, is expected to cover the active site as a lid once the substrate is bound. Perhaps the presence of the phosphate on Ser-193 could somewhat stabilize a more catalytically efficient conformation. We are aware that these effects are shown *in vitro* and no evidence for active site Ser-193 phosphorylation of AADC in a cellular environment has been yet determined. In addition, we realized that phosphomimic substitutions do not reproduce the natural phosphorylated amino acids, even if they are widely used to such scope. Anyway, the value here is to point out that in the context of pathological defects found for AADC, until now overlooked, the possibility for a regulation of AADC by

phosphorylation should be reconsidered for both AADC deficiency variants impaired in folding as well as in catalysis.

Data availability

Data will be made available on request to the corresponding author.

Authors contribution

MB and RSP conceived the study, GB, GR and SC collected data; all authors analyzed and interpreted data; MB and RSP wrote the paper. All authors approved the final version of the manuscript.

Declaration of competing interest

The authors declare the following financial interests/personal relationships which may be considered as potential competing interests. Mariarita Bertoldi reports financial support was provided by PTC Therapeutics Inc. Robert S. Phillips reports financial support was provided by National Institute of General Medical Sciences.

Acknowledgments

The authors would like to thank the skillful technical assistance of Silvia Bianconi (University of Verona) and Chau-wen Chou (Proteomics and Mass Spectrometry Facility, University of Georgia). The contribution of FUR (University of Verona) and PTC Therapeutics IIS2 to MB is gratefully acknowledged. This research was also partially supported by a grant from the National Institute of General Medical Sciences (GM137008) to RSP.

Appendix A. Supplementary data

Supplementary data to this article can be found online at https://doi.org/10.1016/j.bbrc.2023.08.049.

References

[1] M. Bertoldi, Mammalian Dopa decarboxylase: structure, catalytic activity and inhibition, Arch. Biochem. Biophys. 546 (2014) 1–7, https://doi.org/10.1016/j.abb.2013.12.020.

[2] R. Montioli, C.B. Voltattorni, M. Bertoldi, Parkinson's disease: recent updates in the identification of human dopa decarboxylase inhibitors, Curr. Drug Metabol. 17 (2016) 513–518, https://doi.org/10.2174/1389200217051603241705558.

[3] N. Himmelreich, R. Montioli, M. Bertoldi, C. Carducci, V. Leuzzi, C. Gemperle, T. Berner, K. Hyland, B. Thöny, G.F. Hoffmann, C.B. Voltattorni, N. Blau, Aromatic amino acid decarboxylase deficiency: molecular and metabolic basis and therapeutic outlook, Mol. Genet. Metabol. 127 (2019) 12–22, https://doi.org/10.1016/j.ymgme.2019.03.009.

[4] S.P. Craig, A.L. Thai, M. Weber, I.W. Craig, Localisation of the gene for human aromatic L-amino acid decarboxylase (DDC) to chromosome 7p13–>p11 by in situ hybridisation, Cytogenet. Cell Genet. 61 (1992) 114–116, https://doi.org/10.1159/000133384.

[5] M. Krieger, F. Coge, F. Gros, J. Thibault, Different mRNAs code for dopa decarboxylase in tissues of neuronal and nonneuronal origin, Proc. Natl. Acad. Sci. U. S. A. 88 (1991) 2161–2165, https://doi.org/10.1073/pnas.88.6.2161.

[6] H. Ichinose, C. Sumi-Ichinose, T. Ohye, Y. Hagino, K. Fujita, T. Nagatsu, Tissue-specific alternative splicing of the first exon generates two types of mRNAs in human aromatic L-amino acid decarboxylase, Biochemistry 31 (1992) 11546–11550, https://doi.org/10.1021/bi00161a036.

[7] K.L. O'Malley, S. Harmon, M. Moffat, A. Uhland-Smith, S. Wong, The human aromatic L-amino acid decarboxylase gene can be alternatively spliced to generate unique protein isoforms,, J. Neurochem. 65 (1995) 2409–2416, https://doi.org/10.1046/j.1471-4159.1995.65062409.x.

[8] D. Vassilacopoulou, D.C. Sideris, A.G. Vassiliou, E.G. Fragoulis, Identification and characterization of a novel form of the human L-dopa decarboxylase mRNA, Neurochem. Res. 29 (2004) 1817–1823, https://doi.org/10.1023/b:nere.0000042207.05071.ea.

[9] P.I. Artemaki, M. Papatsirou, M.A. Boti, P.G. Adamopoulos, S. Christodoulou, D. Vassilacopoulou, A. Scorilas, C.K. Kontos, Revised Exon Structure of l-DOPA Decarboxylase, Int J Mol Sci 21 (2020), https://doi.org/10.3390/ijms21228568.

[10] S. Millevoi, L. Thion, G. Joseph, C. Vossen, L. Ghisolfi-Nieto, M. Erard, Atypical binding of the neuronal POU protein N-Oct3 to noncanonical DNA targets. Implications for heterodimerization with HNF-3 beta, Eur. J. Biochem. 268 (2001) 781–791, https://doi.org/10.1046/j.1432-1327.2001.01934.x.

[11] C. Dugast, M.J. Weber, NF-Y binding is required for transactivation of neuronal aromatic L-amino acid decarboxylase gene promoter by the POU-domain protein Brn-2, Brain Res Mol Brain Res 89 (2001) 58–70, https://doi.org/10.1016/s0169-328x(01)00063-8.

[12] C. Dugast-Darzacq, S. Egloff, M.J. Weber, Cooperative dimerization of the POU domain protein Brn-2 on a new motif activates the neuronal promoter of the human aromatic L-amino acid decarboxylase gene, Brain Res Mol Brain Res 120 (2004) 151–163, https://doi.org/10.1016/j.molbrainres.2003.10.016.

[13] P.G. Adamopoulos, P. Tsiakanikas, C.K. Kontos, A. Panagiotou, D. Vassilacopoulou, A. Scorilas, Identification of novel alternative splice variants of the human L-DOPA decarboxylase (DDC) gene in human cancer cells, using high-throughput sequencing approaches, Gene 719 (2019), 144075, https://doi.org/10.1016/j.gene.2019.144075.

[14] E. Tremmel, C. Kuhn, T. Kaltofen, T. Vilsmaier, D. Mayr, S. Mahner, N. Ditsch, U. Jeschke, A. Vattai, L-Dopa-Decarboxylase (DDC) is a positive prognosticator for breast cancer patients and epinephrine regulates breast cancer cell (MCF7 and T47D) growth in vitro according to their different expression of G(i)- protein-coupled receptors, Int. J. Mol. Sci. 21 (2020), https://doi.org/10.3390/ijms21249565.

[15] K. Chang, J. Su, C. Li, A. Anwaier, W. Liu, W. Xu, Y. Qu, H. Zhang, D. Ye, Multi-omics profiles refine L-dopa decarboxylase (DDC) as a reliable biomarker for prognosis and immune microenvironment of clear cell renal cell carcinoma, Front. Oncol. 12 (2022), 1079446, https://doi.org/10.3389/fonc.2022.1079446.

[16] M. Hadjiconstantinou, T.A. Wemlinger, C.P. Sylvia, J.P. Hubble, N.H. Neff, Aromatic L-amino acid decarboxylase activity of mouse striatum is modulated via dopamine receptors, J. Neurochem. 60 (1993) 2175–2180, https://doi.org/10.1111/j.1471-4159.1993.tb03503.x.

[17] M.Y. Zhu, A.V. Juorio, I.A. Paterson, A.A. Boulton, Regulation of aromatic L-amino acid decarboxylase by dopamine receptors in the rat brain, J. Neurochem. 58 (1992) 636–641, https://doi.org/10.1111/j.1471-4159.1992.tb09765.x.

[18] M.Y. Zhu, A.V. Juorio, I.A. Paterson, A.A. Boulton, Regulation of striatal aromatic L-amino acid decarboxylase: effects of blockade or activation of dopamine receptors, Eur. J. Pharmacol. 238 (1993) 157–164, https://doi.org/10.1016/0014-2999(93)90843-7.

[19] M.Y. Zhu, A.V. Juorio, I.A. Paterson, A.A. Boulton, Regulation of aromatic L-amino acid decarboxylase in rat striatal synaptosomes: effects of dopamine receptor agonists and antagonists, Br. J. Pharmacol. 112 (1994) 23–30, https://doi.org/10.1111/j.1476-5381.1994.tb13023.x.

[20] E.A. Cartier, L.A. Parra, T.B. Baust, M. Quiroz, G. Salazar, V. Faundez, L. Egaña, G. E. Torres, A biochemical and functional protein complex involving dopamine synthesis and transport into synaptic vesicles,, J. Biol. Chem. 285 (2010) 1957–1966, https://doi.org/10.1074/jbc.M109.054510.

[21] S. Ishikawa, T. Taira, T. Niki, K. Takahashi-Niki, C. Maita, H. Maita, H. Ariga, S. M. Iguchi-Ariga, Oxidative status of DJ-1-dependent activation of dopamine synthesis through interaction of tyrosine hydroxylase and 4-dihydroxy-L-phenylalanine (L-DOPA) decarboxylase with DJ-1, J. Biol. Chem. 284 (2009) 28832–28844, https://doi.org/10.1074/jbc.M109.019950.

[22] R. Tehranian, S.E. Montoya, A.D. Van Laar, T.G. Hastings, R.G. Perez, Alpha-synuclein inhibits aromatic amino acid decarboxylase activity in dopaminergic cells, J. Neurochem. 99 (2006) 1188–1196, https://doi.org/10.1111/j.1471-4159.2006.04146.x.

[23] G. Rossignoli, R.S. Phillips, A. Astegno, M. Menegazzi, C.B. Voltattorni, M. Bertoldi, Phosphorylation of pyridoxal 5'-phosphate enzymes: an intriguing and neglected topic, Amino Acids 50 (2018) 205–215, https://doi.org/10.1007/s00726-017-2521-3.

[24] A.M. Duchemin, M.D. Berry, N.H. Neff, M. Hadjiconstantinou, Phosphorylation and activation of brain aromatic L-amino acid decarboxylase by cyclic AMP-dependent protein kinase, J. Neurochem. 75 (2000) 725–731, https://doi.org/10.1046/j.1471-4159.2000.0750725.x.

[25] A.M. Duchemin, N.H. Neff, M. Hadjiconstantinou, Aromatic L-amino acid decarboxylase phosphorylation and activation by PKGIalpha in vitro, J. Neurochem. 114 (2010) 542–552, https://doi.org/10.1111/j.1471-4159.2010.06784.x.

[26] R. Montioli, G. Bisello, M. Dindo, G. Rossignoli, C.B. Voltattorni, M. Bertoldi, New variants of AADC deficiency expand the knowledge of enzymatic phenotypes, Arch. Biochem. Biophys. 682 (2020), 108263, https://doi.org/10.1016/j.abb.2020.108263.

[27] E. Peterson, H. Sober, Preparation of crystalline phosphorylated derivatives of vitamin B6, J. Am. Chem. Soc. 76 (1954) 169–175.

[28] F.W. Studier, Protein production by auto-induction in high density shaking cultures, Protein Expr. Purif. 41 (2005) 207–234, https://doi.org/10.1016/j.pep.2005.01.016.

[29] W.M. Yonemoto, M.L. McGlone, L.W. Slice, S.S. Taylor, Prokaryotic expression of catalytic subunit of adenosine cyclic monophosphate-dependent protein kinase, Methods Enzymol. 200 (1991) 581–596, https://doi.org/10.1016/0076-6879(91)00173-t.

[30] A.F. Sherald, J.C. Sparrow, T.R. Wright, A spectrophotometric assay for Drosophila dopa decarboxylase,, Anal. Biochem. 56 (1973) 300–305, https://doi.org/10.1016/0003-2697(73)90194-2.

[31] A. Charteris, R. John, An investigation of the assay of dopamine using trinitrobenzensulphonic acid, Anal. Biochem. 66 (1975) 365–371, https://doi.org/10.1016/0003-2697(75)90604-1.

[32] G. Rossignoli, A. Grottesi, G. Bisello, R. Montioli, C. Borri Voltattorni, A. Paiardini, M. Bertoldi, Cysteine 180 is a redox sensor modulating the activity of human

pyridoxal 5'-phosphate histidine decarboxylase, Biochemistry 57 (2018) 6336–6348, https://doi.org/10.1021/acs.biochem.8b00625.
[33] M. Bertoldi, P. Frigeri, M. Paci, C.B. Voltattorni, Reaction specificity of native and nicked 3,4-dihydroxyphenylalanine decarboxylase, J. Biol. Chem. 274 (1999) 5514–5521, https://doi.org/10.1074/jbc.274.9.5514.
[34] M. Bertoldi, S. Castellani, C. Bori Voltattorni, Mutation of residues in the coenzyme binding pocket of Dopa decarboxylase. Effects on catalytic properties, Eur. J. Biochem. 268 (2001) 2975–2981, https://doi.org/10.1046/j.1432-1327.2001.02187.x.
[35] P. Burkhard, P. Dominici, C. Borri-Voltattorni, J.N. Jansonius, V.N. Malashkevich, Structural insight into Parkinson's disease treatment from drug-inhibited DOPA decarboxylase, Nat. Struct. Biol. 8 (2001) 963–967, https://doi.org/10.1038/nsb1101-963.
[36] M. Bertoldi, M. Gonsalvi, R. Contestabile, C.B. Voltattorni, Mutation of tyrosine 332 to phenylalanine converts dopa decarboxylase into a decarboxylation-dependent oxidative deaminase, J. Biol. Chem. 277 (2002) 36357–36362, https://doi.org/10.1074/jbc.M204867200. M204867200 [pii].
[37] R. Montioli, M. Dindo, A. Giorgetti, S. Piccoli, B. Cellini, C.B. Voltattorni, A comprehensive picture of the mutations associated with aromatic amino acid decarboxylase deficiency: from molecular mechanisms to therapy implications,, Hum. Mol. Genet. 23 (2014) 5429–5440, https://doi.org/10.1093/hmg/ddu266.
[38] R. Montioli, A. Paiardini, M.A. Kurian, M. Dindo, G. Rossignoli, S.J.R. Heales, S. Pope, C.B. Voltattorni, M. Bertoldi, The novel R347g pathogenic mutation of aromatic amino acid decarboxylase provides additional molecular insights into enzyme catalysis and deficiency, Biochim. Biophys. Acta 1864 (2016) 676–682, https://doi.org/10.1016/j.bbapap.2016.03.011.
[39] H. Komori, Y. Nitta, H. Ueno, Y. Higuchi, Structural study reveals that Ser-354 determines substrate specificity on human histidine decarboxylase, J. Biol. Chem. 287 (2012) 29175–29183, https://doi.org/10.1074/jbc.M112.381897.
[40] A. Tramonti, D. De Biase, A. Giartosio, F. Bossa, R.A. John, The roles of His-167 and His-275 in the reaction catalyzed by glutamate decarboxylase from Escherichia coli,, J. Biol. Chem. 273 (1998) 1939–1945, https://doi.org/10.1074/jbc.273.4.1939.
[41] G. Bisello, K. Kusmierska, M.M. Verbeek, J. Sykut-Cegielska, M.A.A.P. Willemsen, R.A. Wevers, K. Szymańska, J. Poznanski, J. Drozak, K. Wertheim-Tysarowska, A. M. Rygiel, M. Bertoldi, The novel P330L pathogenic variant of aromatic amino acid decarboxylase maps on the catalytic flexible loop underlying its crucial role, Cell. Mol. Life Sci. 79 (2022) 305, https://doi.org/10.1007/s00018-022-04343-w.
[42] P.S. Moore, M. Bertoldi, P. Dominici, C. Borri Voltattorni, Aromatic amino acid methyl ester analogs form quinonoidal species with Dopa decarboxylase, FEBS Lett. 412 (1997) 245–248, https://doi.org/10.1016/s0014-5793(97)00788-6.
[43] H.C. Dunathan, Conformation and reaction specificity in pyridoxal phosphate enzymes, Proc. Natl. Acad. Sci. U. S. A. 55 (1966) 712–716.
[44] M. Bertoldi, B. Cellini, B. Maras, C.B. Voltattorni, A quinonoid is an intermediate of oxidative deamination reaction catalyzed by Dopa decarboxylase,, FEBS Lett. 579 (2005) 5175–5180, https://doi.org/10.1016/j.febslet.2005.08.029. S0014-5793(05)01014-8 [pii].
[45] M. Bertoldi, B. Cellini, R. Montioli, C. Borri Voltattorni, Insights into the mechanism of oxidative deamination catalyzed by DOPA decarboxylase, Biochemistry 47 (2008) 7187–7195, https://doi.org/10.1021/bi800478s.
[46] R.A. John, Pyridoxal phosphate-dependent enzymes, Biochim. Biophys. Acta 1248 (1995) 81–96, 0167–4838(95)00025-P [pii].
[47] R.S. Phillips, Chemistry and diversity of pyridoxal-5'-phosphate dependent enzymes, Biochim. Biophys. Acta 1854 (2015) 1167–1174, https://doi.org/10.1016/j.bbapap.2014.12.028.
[48] M. Bertoldi, C. Borri Voltattorni, Reaction of dopa decarboxylase with L-aromatic amino acids under aerobic and anaerobic conditions, Biochem. J. 2 (2000) 533–538, 352 Pt.